ORIGINAL RESEARCH ARTICLE

Grain Coarsening of Columnar Iron Polycrystals by Repetitive Cold Work and Annealing

JAKUB HOLZER, MIROSLAV HUSŤÁK, JITKA HEGROVÁ, and ROMAN GRÖGER

Experimental studies on single crystals of pure metals are essential for understanding the mechanisms governing their plastic deformation as well as for interpretations of these observations using theoretical and atomistic models. Iron is especially interesting, because its low-temperature plastic response may be affected by ferromagnetism. However, the growth of large single crystals of iron from the melt is notoriously difficult due to the allotropic transformation between its face-centered and body-centered cubic phases. An alternative route is to start with polycrystalline iron of high purity and subject it to one or more cycles of cold work and subsequent annealing. This process is demonstrated here by utilizing 99.99 pct pure polycrystalline electrolytic iron with initially strong columnar microstructure. We investigate how the final grain size depends on the number of cold work cycles, annealing time in vacuum, and annealing temperature. The size distribution and characters of individual grains are assessed on etched samples using the electron backscatter diffraction analysis. The largest grains obtained by this process have the characteristic sizes above 2 mm and require four cycles of cold work, each followed by annealing at 870 °C for 8 hours. The probability density of grain sizes after optimal combination of cold work and annealing is well approximated by log-normal distribution. These results constitute guidelines to optimal processing of columnar polycrystals for further extraction of single-crystalline samples.

https://doi.org/10.1007/s11661-022-06866-0

I. INTRODUCTION

EXPERIMENTAL studies of the mechanisms of plastic deformation in iron require very pure materials either in single crystal form or as polycrystals with grains sufficiently large so as to allow extraction of test samples representative of the bulk. Preparation of large single crystals of iron is possible either directly by drawing an oriented rod from a molten metal or by recrystallization of polycrystalline iron in solid state. When preparing a material from the melt, the initial crystallization into the body-centered cubic (bcc) δ-phase and subsequently into the face-centered cubic (fcc) γ-phase (austenite) leads to high solubility of small oxygen, carbon and nitrogen atoms that act as interstitial solutes occupying large tetrahedral and octahedral sites.[1] Upon further cooling into the body-centered cubic α-iron (ferrite), these interstitials are found primarily in smaller octahedral sites, where they partially relieve the misfit strain. However, their stability in the host ferrite lattice makes it difficult to further purify the material in solid state by the process of zone refinement. The typical concentration of residual impurities is around 60 ppm with 10 ppm of non-metallic impurities.[2] Due to the difficulties in achieving uniform heat distribution through the thickness of the specimen, this process is typically used to produce rods with diameters only up to a few millimeters.

Much larger single crystals of iron can be produced by a combination of mechanical and thermal treatment provided the right conditions are met. In particular, it has been shown in a number of experiments first on aluminum, molybdenum, and tungsten since the 1920s that a small amount of cold work does not lead to any grain growth.[3] Above a certain critical strain, the plastic deformation is stored nearly uniformly in the interiors of grains and can activate the migration of grain boundaries during subsequent annealing. The driving force for recrystallization is provided by the strain energy stored during cold work around excess dislocations and point defects.[4] In this process, a large number of non-equilibrium grains grow at the expense of a few which received the least amount of strain. However, once the storage capacity of individual grains

JAKUB HOLZER, MIROSLAV HUSŤÁK, and ROMAN GRÖGER are with the Institute of Physics of Materials and CEITEC IPM, Czech Academy of Sciences, Žižkova 22, 616 00 Brno, Czech Republic. Contact e-mail: holzer@ipm.cz JITKA HEGROVÁ is with the Transport Research Centre, Líšeňská 33a, 636 00 Brno, Czech Republic.
Manuscript submitted June 6, 2022; accepted September 29, 2022.
Article published online December 5, 2022

is exceeded, further increase of the amount of cold work does not lead to larger grains. The excess strain energy is then deposited exclusively at grain boundaries from which new crystals grow during thermal treatment. It is thus imperative that the right amount of cold work is applied to turn polycrystalline iron into its single crystal form. Indeed, it was observed already by Antonione *et al.*[5] that the strain anneal method produces larger grain sizes in less deformed samples. The critical stress to initiate the abnormal grain growth is not fixed but increases with increasing grain size,[4] which means that larger deformation is needed to produce the critical microstructure as the grains become bigger. Even with the ideal procedure at hand, the success in producing a single crystal decays rapidly with increasing sample size.

The application of this procedure to recrystallization of polycrystalline iron originally in the form of equiaxed grains was first made by Kadečková and Šesták.[6] They have demonstrated that grains of millimeter size can be produced by several cycles of cold work and subsequent annealing. The dislocation density near the growth front was much lower than in the as-grown crystal, which indicates that most dislocations are generated by thermal and other stresses within the grains.[7] Kranzlein *et al.*[8] have used the strain anneal method (straining 3 pct in tension at the strain rate of $7 \times 10^{-5}\,s^{-1}$) by utilizing a custom design of their gradient furnace to produce highly pure single crystals of iron 80 pct of the time. By testing their samples in tension at temperatures between − 196 °C and 20 °C they have demonstrated the change in the mechanism of plastic deformation from pure slip at high temperatures to a combination of slip and twinning at − 196 °C. A similar strain anneal procedure was used by Rosinger *et al.*[9] who reported 80 pct success in obtaining cylindrical iron single crystals from equiaxed grains that were first strained 3 pct at the strain rate of $3.3 \times 10^{-5}\,s^{-1}$ and then drawn through the temperature gradient with the maximum temperature of 870 °C. In order to prevent the formation of carbides, their samples were quenched rather than slowly annealed. Tomalin and McMahon Jr[10] have demonstrated that adding nitrogen leads to 60 to 70 pct success in producing single crystals. A modification of the growth procedure was proposed by Bailey and Brewer,[11] where the crystal was pulse-heated by repetitively increasing the temperature to 870 °C and cooling below 750 °C. This suppressed the random nucleation of new grains ahead of the growth interface and resulted in very large grains. Lubitz and Göltz[12] succeeded in preparing large spherical iron single crystals using the critical strain of 3.3 pct and moving the rod through a water-cooled jacket that was heated to 890 °C. Most recently, the technique of strain-induced abnormal grain growth was used by Jin *et al.*[13] to produce grains of 1 cm × 2.2 cm but in foils of only 50 μm recently shown that precipitates thickness. Almeida *et al.*[14] have greatly reduce the chance of obtaining a uniform distribution of large grains. After primary recrystallization of their cold-drawn iron wire with the diameter of 300 μm at 1123 K, many precipitates were found close to the wire's surface where no grain growth was observed. The abnormal grain growth took place exclusively in the central part of the wire, but the grains could not reach the surface. The reverse process of growing large columnar grains from nearly equiaxed grains is possible using directional annealing as was demonstrated recently by Zhang *et al.*[15]

Our objective in this paper is to revisit the methodology pioneered in Reference 6 to investigate the optimal conditions needed to transform a highly oriented columnar microstructure of electrolytic iron into a polycrystal with large equiaxed grains. In particular, we determine the right amount of strain that has to be applied at room temperature, for which the subsequent thermal treatment leads to initiation of rapid grain growth. We further study the number of cold work cycles and annealing that produce the largest grains. Electron backscatter diffraction (EBSD) analysis is employed to assess the sizes the orientations of individual grains. These data are further used to describe the probability densities of grain sizes using suitable distribution functions.

II. EXPERIMENTAL PROCEDURE

The source material was electrolytic iron of 99.99 pct purity acquired from Blyth Metals Ltd., UK. The chemical composition was investigated using the ICP/MS spectrometer Agilent 8800 Triple Quad at the Transport Research Centre Brno. The major inorganic impurities (> 1 wt ppm) were Mg (≤ 16.6), Ca (≤ 10.7), K (≤ 8.92), S (≤ 8.11), Al (7.3), Cu (≤ 5.97), Na (≤ 3.38), Se (≤ 1.94), Si (≤ 1.44), Cr (1.39), Zn (≤ 1.29), where the values with inequalities are below the detection limit of the ICP/MS method, and thus constitute upper bounds of their concentrations. The as-received samples were in the form of flat pieces with irregular shapes, thicknesses ranging from 5 to 7 mm, and the lateral sizes from 10 to 20 mm.

The initial microstructure of the as-received material consisted of long columnar grains oriented perpendicular to its flat planes, as shown in Figure 1. No thermal or mechanical treatment was performed before extracting the test samples. Seven cuboidal samples of approx. 4 mm × 4 mm × 12 mm were cut out such that the columnar grains were aligned perpendicular to one side (marked A) and parallel to another (marked B). They were first ground mechanically using the sandpapers of

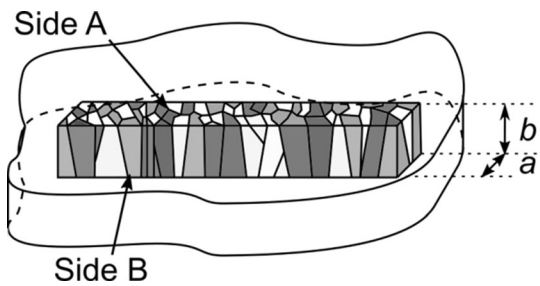

Fig. 1—The source material and the extracted test sample showing the initial orientations of grains.

80, 220, 600 and 1200 grit size and then polished on a polishing cloth using the diamond paste with particle sizes of 3 and 1 μm. To remove the damaged surface layer, the samples were then etched either in 10 pct Nital solution for 7 seconds or in the Struers™ A3 etching electrolyte. The precise conditions for each sample are specified in Table I. The distribution of sizes and orientations of grains in individual samples were investigated by the EBSD analysis using the scanning electron microscope TESCAN Lyra 3 XMU FEG/SEMxFIB equipped with the Symmetry EBSD camera from Oxford Instruments. The EBSD maps were acquired using the Aztec software from Oxford Instruments. All EBSD maps presented here were acquired at the accelerating voltage of 20 keV, approx. 12 nA probe current, working distance of 12 mm, step size of 10 μm, and the exposure time of 0.3 milliseconds. The hit rate (percentage of indexed points) of acquired maps was around 90 pct. However, this percentage is higher in reality, as the scans were slightly larger than the specimen and thus there is a rim of unindexed points around the specimen. No data correction was performed for the grain analysis except for removing grains smaller than four pixels that constitute errors in the indexation.

The sample MH1 represents the as-received state of the material. It was neither deformed nor annealed, only prepared for microscopic evaluation by the procedure outlined above. The EBSD maps taken from the sides A and B of the sample MH1 after etching in the A3 electrolyte with the current density of 1.18 A cm^{-2} are shown in Figures 2(a) and (b), respectively. Figure 2(a) is a projection of the columnar grains along their long axis, which reveals more or less polyhedral characters of their cross-sections. Figure 2(b) is the projection in the direction perpendicular to these grains, which exposes their columnar character. Here, it is easy to recognize two different grains even if their orientations are quite similar. The grain boundaries do not produce any EBSD signal and, therefore, the boundary between two different grains with similar orientations is clearly discernible. The average grain size as computed from the EBSD analysis on both sides of the sample MH1 was (165 ± 145) μm. Because this sample did not undergo any mechanical or thermal treatment, the microstructure shown in Figure 2 is used as a reference toward which the microstructures of all other samples are compared. All further EBSD maps in this article are presented using the same imaging conditions, *i.e.*, the side A is shown in the inverse pole figure (IPF) Z projection, and the side B in the IPF Y projection. The fitted ellipse aspect ratio (FEAR) of the initial microstructure shown in Figures 2(a) and (b) is 2.01 and 4.26.

The samples MH3, MH4 and MH5 first underwent about 5 pct compression at room temperature using a hand press in both directions perpendicular to the long axes of the samples, where one such direction was parallel and the other perpendicular to the initial columnar grains. The total plastic strain produced in this way along the grains was around 10 pct. The samples were then individually sealed in three quartz tubes under vacuum conditions, annealed at 870 °C for 6 hours (sample MH3), 8 hours (sample MH4), and 10 hours (sample MH5) and quenched into water. This annealing temperature was considered previously by Kadečková and Šesták[6] as the highest temperature to avoid transformation into the fcc phase. After annealing for 6 hours, the sample MH3 had the average grain size of (248 ± 180) μm. The annealing time of 8 hours used for the sample MH4 resulted in the average grain size of (270 ± 149) μm. Prolonging the annealing time by 2 hours compared to MH3 thus increased the grain size by 22 μm. Further increase of the annealing time to 10 hours, as considered for the sample MH5, did not show any further grain growth; the resulting grain size was (269 ± 198) μm. In the following studies, we have thus considered 8 hours as the optimal time for annealing the samples in vacuum at 870 °C. The microstructure of the sample MH4 obtained by this annealing procedure is shown in Figure 3. Compared with the as-received state MH1, shown in Figure 2, the columnar character of individual grains is almost lost in Figure 3, and the grains transformed into nearly equiaxed shapes. Moreover, the side B of this sample, shown in Figure 3(b), displays a number of very large grains with characteristic sizes in excess of 1 mm.

After a single cycle of compression and annealing, the sample MH3 had a larger average grain size, as shown later in the text in Figure 5(a). Smaller grains were often found lodged into larger ones, but they disappeared with increasing number of thermomechanical cycles. In the samples that underwent more cycles of cold work and annealing, smaller grains were often found at grain boundaries, or they were clustered together. In the following, the microstructure of sample MH4 obtained after one cycle of cold work followed by annealing under the optimal conditions was taken as the reference state. The three remaining samples (MH6, MH7, MH8) were used to study how the grains grow upon a repeated application of cold work at room temperature and annealing under the same conditions as MH4. In particular, the sample MH6 underwent two cycles of cold work and subsequent annealing, MH7 three of these cycles, and MH8 four such cycles. The details of this procedure are given in Table I, including the dimensions of each sample and information about the sample treatment. During each annealing step, several large grains grew at the expense of many small surrounding grains. Quantitative estimates of the average grain sizes are less relevant since the goal was to produce as large grains as possible at the expense of other grains. Instead, the samples were characterized by the largest grain in both directions parallel and perpendicular to the initial columnar grains. The grains with the largest area in the sample MH6 had the area of 0.285 mm^2 (side A) and 0.408 mm^2 (side B). The largest grains in the sample MH7 had the area of 0.44 mm^2 (side A) and 0.946 mm^2 (side B). The grains in the sample MH8 were the largest of all three samples with the area of 4.102 mm^2 (side A) and 6.296 mm^2 (side B).

The elongations of grains in the initial state (MH1) vanished entirely after two thermomechanical cycles, *i.e.*, in samples MH6, MH7, and MH8. A significant increase in the largest grain area was observed in sample

Table I. Dimensions of Individual Samples and Their Combined Mechanical and Thermal Treatment

	MH1		MH3		MH4		MH5	
Initial Size	*a* (mm)	*b* (mm)	*a* (mm)	*b* (mm)	*a* (mm)	*b* (mm)	*a* (mm)	*b* (mm)
	3.810	3.670	4.240	4.271	4.071	4.068	3.890	3.940
Deformation (Pct)	no deformation		5.1	4.5	5.9	4.4	4.4	6.6
Annealing	no annealing		870 °C, 6 hours		870 °C, 8 hours		870 °C, 10 hours	
Etchant	A3 electrolyte, current density $J = 1.18$ A cm^{-2}				10 pct nital, 7 seconds			

	MH6		MH7		MH8	
Initial Size	*a* (mm)	*b* (mm)	*a* (mm)	*b* (mm)	*a* (mm)	*b* (mm)
	3.794	4.077	3.912	4.106	4.143	3.990
1st Deformation (Pct)	5.5	5.2	4.2	5.6	5.1	5.1
Annealing			870 °C, 8 hours			
2nd Deformation (Pct)	6.0	5.0	8.0	5.0	4.0	6.0
Annealing			870 °C, 8 hours			
3rd Deformation (Pct)	—	—	6.0	4.0	4.0	7.0
Annealing	—				870 °C, 8 hours	
4th Deformation (Pct)	—	—	—	—	9.5	9.3
Annealing	—		—		870 °C, 8 hours	
Etchant	10 pct nital, 7 seconds				A3 electrolyte, current density $J = 1.18$ A cm^{-2}	

MH1 is the reference sample (no deformation and no thermal treatment). MH3, MH4, MH5 were used to investigate annealing times. MH6, MH7, MH8 served to determine the optimal number of cold work cycles. Sample MH2 contained large voids and was excluded from the analysis.

MH8 that underwent four cycles of cold work and annealing as compared to sample MH7 with only three such cycles. This may be, at least partially, attributed to differences in the plastic strain applied during cold work. In particular, as Table I shows, the final state of sample MH7 was produced by about 5 pct compression as judged by averaging the plastic strain measured from the changes of the sample widths *a* and *b*. It should be emphasized that the last compression exerted on sample MH8 was over 9 pct. The EBSD analysis of sample MH8, shown in Figure 4, suggests that four cycles of cold work and annealing result in grains with characteristic sizes in excess of 2 mm. However, this final microstructure still contains a large number of small grains. If need be, these residual grains can be removed by additional cycles of cold work and annealing. Due to increasing grain size, a great care would have to be exercised in this process to avoid exceeding the critical strain for which new dislocations start nucleating at the boundaries of smaller grains.

While the sizes of individual grains are not easily accessible, a number of approximations have been developed over the years[16,17] based on cross-sections of a large number of grains by one or more sample surfaces. Here, we observe that grains in most samples after mechanical and thermal treatment are close to being equiaxed, which permits the approximation of their volumes by equivalent spheres as used in Reference 6. However, only planar cuts of these grains (*i.e.*, also approximating spheres) are observed on the surface, which project individual grains as circular areas with diameters *d*. Measuring the projected area of the *i*th grain, A_i, allows to determine the diameter of this circle as

$$d_i = \sqrt{4A_i/\pi}. \quad [1]$$

This calculation has to be done for many (N) grains on both sides A and B, and the resulting diameters d_i combined to obtain the average diameter $\overline{d} = (\sum_{i=1}^{N} d_i)/N$. We then define the average (effective) grain by a sphere with diameter $\overline{d}$. The variation of these average grain sizes for different samples (*i.e.*, different annealing times) are shown in Figure 5(a). Most of our samples contained equiaxed grains for which the approximation above is justified. However, it is not appropriate for the columnar grains observed in the reference sample MH1, where the representation of grains by spheres results in a large standard deviation of the average grain size. As the annealing time for samples MH3–5 increases, the grains become quickly equiaxed. The sample MH5 shows a slightly smaller average grain size compared to sample MH4, which may have been caused by reaching steady state for the amount of cold work applied (see Table I). This was caused by the appearance of clusters of small grains, which somewhat lowered the average grain size even though other grains were slightly bigger than those in sample MH4. The standard deviation of $\overline{d}$ further increased in samples that underwent multiple deformation-annealing cycles, which is probably caused by the presence of large grains. These grew at the expense of smaller ones, thus broadening the distributions of grain sizes. However, it is more important that the effective grain size gradually

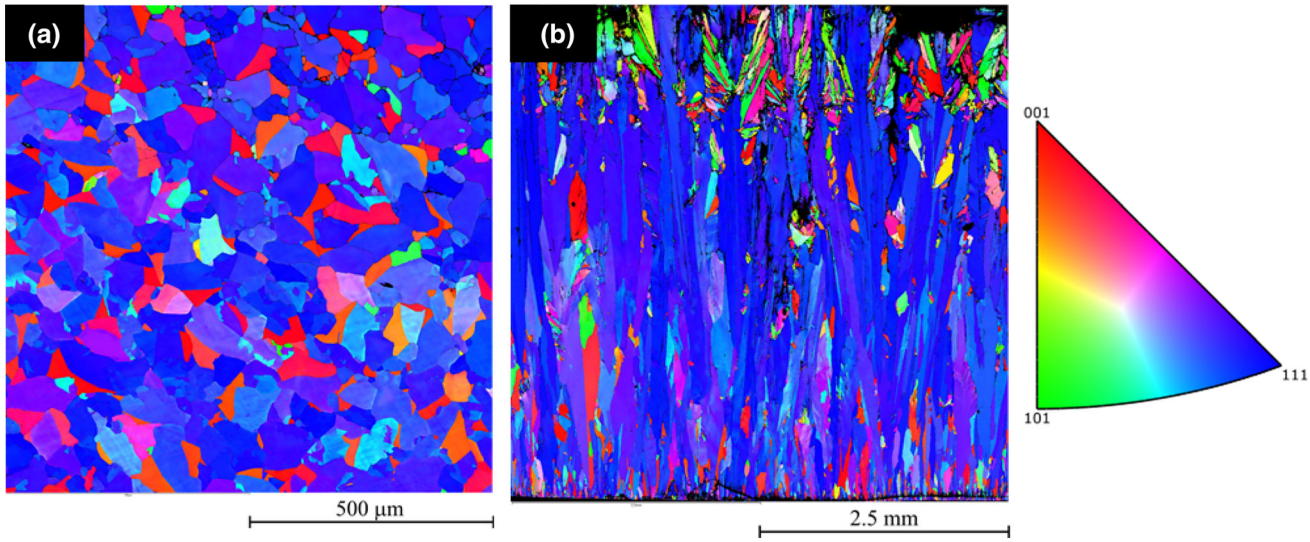

Fig. 2—Microstructure of the as-received 99.99 pct pure electrolytic iron (reference sample MH1) taken with the use of the EBSD mode in SEM, where each color represents a different local orientation of the crystal lattice: (*a*) image taken parallel to the long axis of columnar grains (side A) is shown in the IPF Z projection, and (*b*) image taken perpendicular to the columnar grains (side B) is shown in the IPF Y projection (Color figure online).

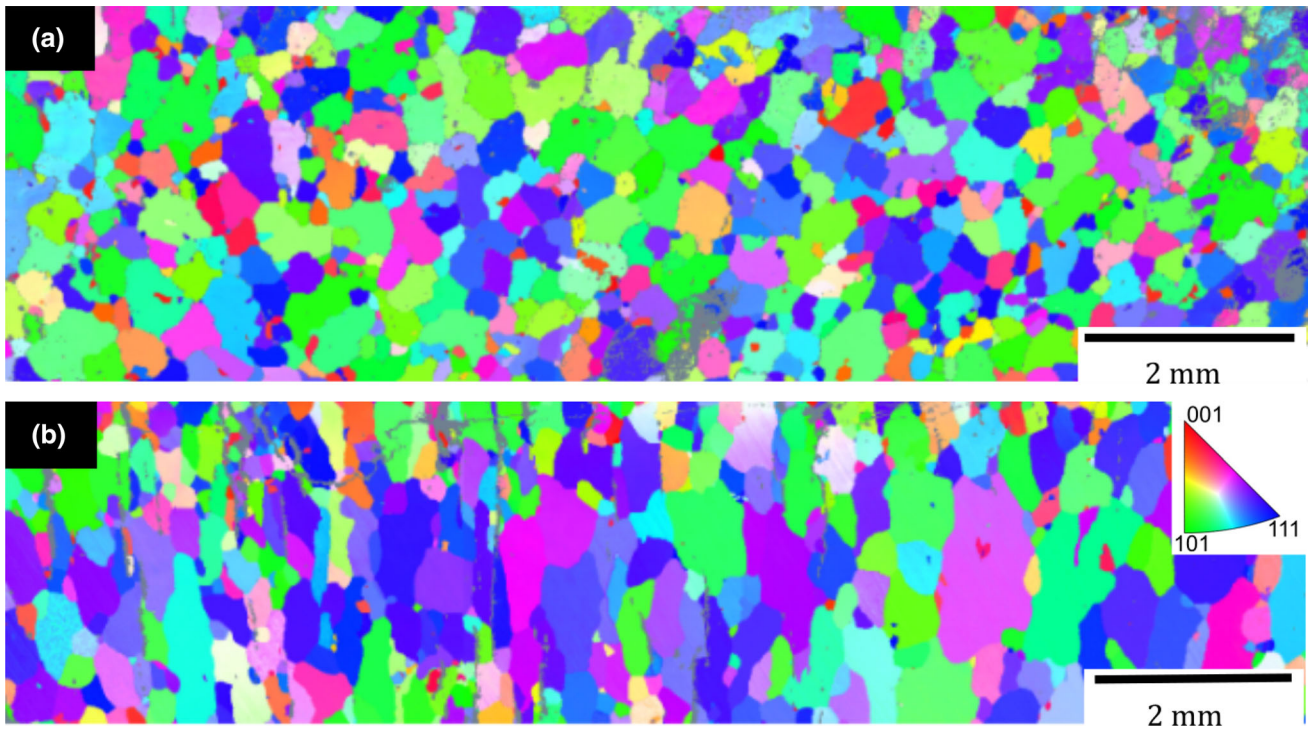

Fig. 3—Microstructure of the sample MH4 obtained after one cycle of cold work at room temperature and optimal annealing time of 8 hours in vacuum at 870 °C. The image (*a*) is taken from side A (IPF Z projection) and the image (*b*) from side B (IPF Y projection).

increases with the cumulative annealing time as shown in Figure 5(a) for samples MH6, MH7 and MH8 that underwent two, three and four cycles of cold work and annealing, respectively.

For the purpose of presentation in Figure 5(a), we consider only the cumulative annealing time for each sample, which is a sum of the annealing times taken in all cycles. For the samples MH6–8, the standard deviation increased with the number of cycles even though the average grain sizes on both sides A and B were fairly similar (in contrast to samples MH3–5). Instead, the large standard deviations of $\overline{d}$ on samples MH6–8 come from differences between grain sizes observed on each side. This is evident from Figure 4,

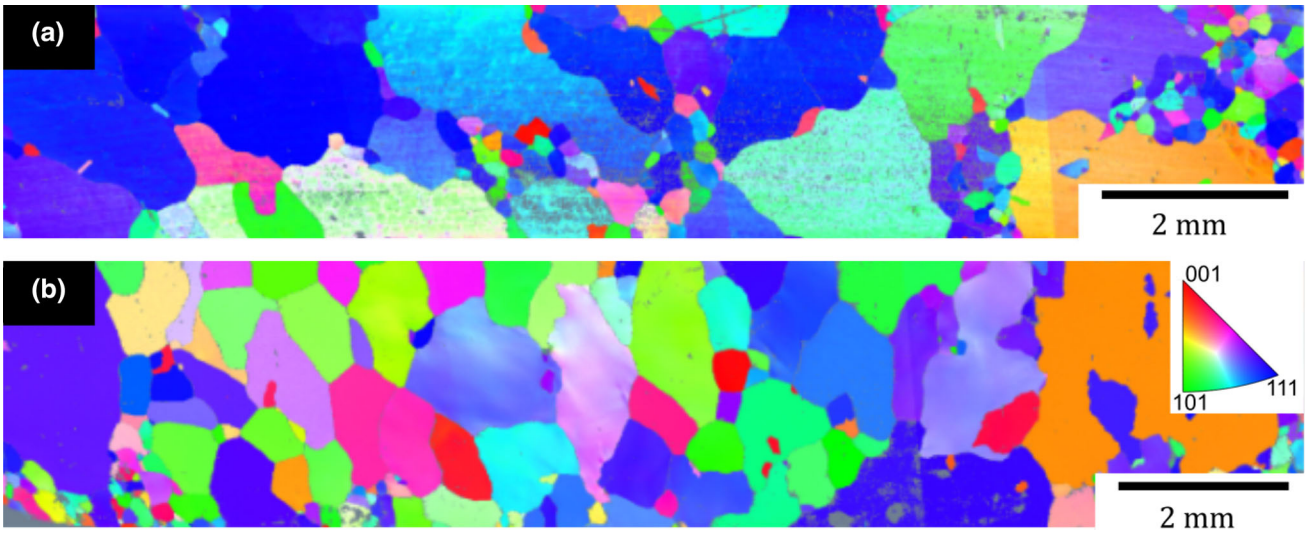

Fig. 4—Microstructure of the sample MH8 with the largest grains obtained in this work: (*a*) image taken from side A (IPF Z projection), and (*b*) from side B (IPF Y projection).

where one can easily find very large grains next to a cluster of several small grains. Figure 5(a) also shows a comparison of our statistical data with those of Kadečková and Šesták[6] obtained on circular rods whose diameters were reduced by 20 pct. Their results show rapid increase of the grain size within the first 100 minutes of annealing, followed by a much more gradual increase within the next 900 minutes. Our results in Figure 5(a) show that multiple cycles of compression and subsequent annealing result in even further increase of the grain size. To complete the statistical analysis of grain size distributions in our samples, we plot in Figure 5(b) the dependence of the grain area observed on sides A, B of each sample on the cumulative plastic strain ϵ. The latter is defined as the sum of individual plastic strains ϵ_i applied on the sample in each of its deformation cycle i. Specifically, $\epsilon = \sum_i \epsilon_i$, where $\epsilon_i = (l - l_0)/l_0$, where l_0 is the thickness of the sample in one of the two directions perpendicular to the long axis before each mechanical and thermal treatment cycle (*i.e.*, $l = a$ or b as shown in Table I). Some of the grains have their characteristic diameters larger than 1 mm and areas of several mm^2. These grains were easily recognizable even with a naked eye once the sample was polished and etched. Because the sample MH8 with most cycles contained a large number of small grains, it is questionable whether further deformation-annealing cycles would increase the average grain size. The presence of small grains may have been caused by extensive plastic deformation, where the newly nucleated dislocations were not stored entirely inside large grains.

In Figure 6, we plot the IPFs taken from samples MH1, MH4 and MH8, which show the changes in grain orientations during the combined mechanical and thermal treatment, as explained in the previous text. Figures 6(a) and (d) shows strong crystallographic texture in the initial state without any treatment (MH1), where most grains have orientations parallel to ⟨111⟩. A single cycle of cold work followed by 8 hours annealing leads to a reorientation of grain sizes, as shown in Figures 6(b) and (e) for sample MH4. Here, the most probable grain orientation is different on the size A (deviation toward ⟨110⟩) and on the side B (deviation toward ⟨001⟩). The optimal combination of the number of cold work and annealing cycles, as considered for the sample MH8, does not lead to stronger homogenization of grain orientations. Instead, the primary effect is to change the mean grain orientation, as shown for the two sides in Figures 6(c) and (f). However, it should be emphasized that these maps were taken only from about 1/3 of the sample surface. In the case of MH1 and MH4, this area still contains a large number of grains that produce a reliable statistics of grain orientations. However, the same area on the sample MH8 contains much fewer grains whose orientations thus dominate the statistics. Nonetheless, the trend shown in Figure 6 suggests that the proposed combination of mechanical and thermal treatment leads not only to grain growth but also to homogenization of the orientations of individual grains.

III. RESULTS AND DISCUSSION

In the following, we will employ the linear intercept method of Smith and Guttman[18] to characterize grain size distributions in annealed samples. This method is based on randomly placing a line of length L over the microstructure and counting the number of its intersections (N) with grain boundaries (the end points are counted as 1/2 each). The mean chord length is then obtained as $\bar{l} = L/N$. The calculation of $\bar{l}$ can be done routinely from surface micrographs and does not involve any assumption about the grain shape. As pointed out by Thompson,[19] $\bar{l}$ does not represent the true characteristic size of the grain (*e.g.*, a diameter in case of the approximation by spheres), because surface

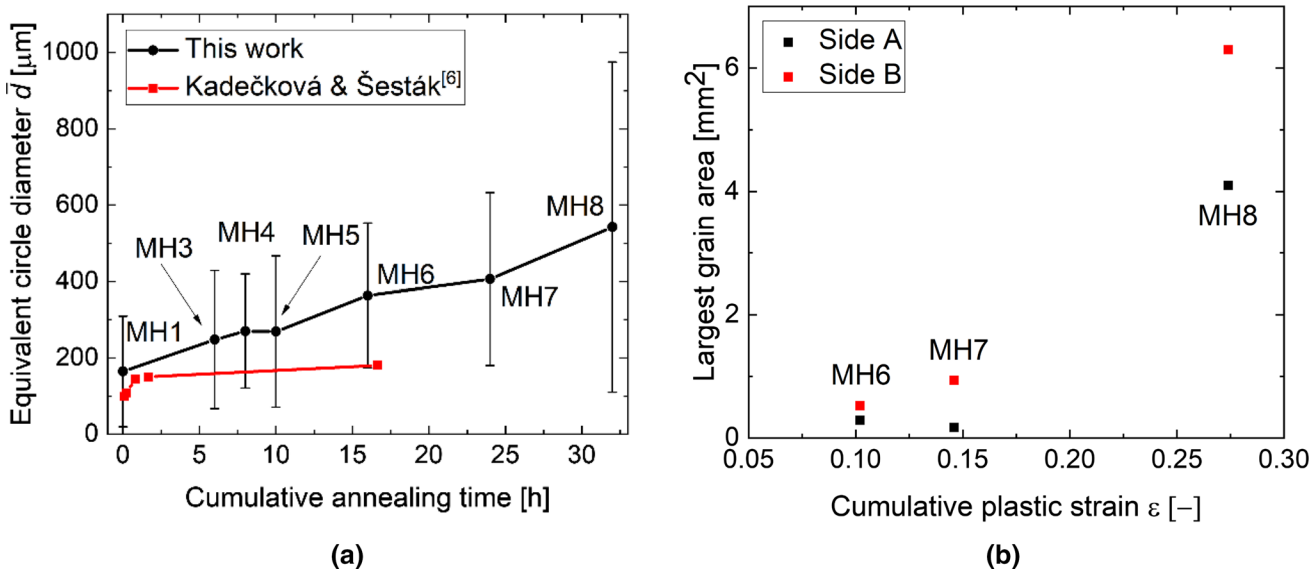

Fig. 5—(*a*) Dependence of the equivalent circle diameter $\bar{d}$ on the cumulative annealing time (for comparison, we also show the results obtained earlier in Ref. [6]). (*b*) Variation of the largest grain area measured on the sides A and B of each sample with the amount of cumulative plastic strain.

cuts are almost never made through the centers of grains. The largest deviation between $\bar{l}$ and the true diameter of the grain ($\bar{d}$) is obtained for an approximation of grains by spheres with uniform diameters that gives $\bar{d} = 1.5\bar{l}$ [20] or $\bar{d} = 1.62\bar{l}$, [21] depending on the method of sectioning. A more physically appealing approach is to describe the grains by Kelvin cells with six flat quadrilateral and eight hexagonal faces for which the conversion is $\bar{d} = 1.68\bar{l}$. [22] Further advancements of these correlations can be found in Reference 19. The correspondence between grain sizes determined from surface (planar) measurements and spatial measurements was confirmed to be very good for equiaxed grains.[23,24] Despite very different assumptions about the grain shape, the range of coefficients from 1.5 to 1.68 is rather narrow. For the purpose of deducing the grain size distributions from their planar sections, the convexity of grains thus seems more important than their precise shapes.

Within the linear intercept method, the average grain volume V_g may be calculated from planar projections of the microstructure given the grains are not too elongated in any direction. If this process is repeated for many random orientations of the line, the average grain volume may be closely approximated as[18]

$$V_g = \frac{4}{\pi \bar{l}} \left(\frac{A}{M} \right)^2, \qquad [2]$$

where A is the surface area of the specimen, M the number of grains inside this region, and $\bar{l}$ was defined above. The characteristic grain size can be either obtained directly from Eq. [2] as $d = (6V_g/\pi)^{1/3}$ or as the average length of linear intercepts from $\bar{d} = 1.68\bar{l}$. These calculations were made by considering a large number of randomly oriented lines for which the two diameters were determined using our Python script. The results obtained on samples MH4 (best sample after optimization of thermal treatment) and MH8 (final sample after combined thermal and mechanical treatment) are shown in Table II. The average grain volumes calculated from the EBSD maps on samples MH4 and MH8 are summarized in Table II. Even after many cycles of cold work and annealing, the initially columnar character of grains is still evident from different values of V_g obtained from the sides A and B. For both samples, the calculations made on side B with initially elongated grains produce larger V_g than the calculations made on side A with initially nearly equiaxed projections of grains. The grain volume averaged from both sides has increased by 95 pct from MH4 to MH8. Similar arguments as above hold also for the two characteristic grain diameters d and $\bar{d}$. While both these methods give slightly different approximations of the characteristic grain size, the trend is the same in both cases.

In Figures 7(a) and (b), we plot the histograms of chord lengths representing the distances between two successive line intersections with grain boundaries on samples MH4 and MH8, respectively. For both samples, the measurements made on sides A and B were combined into a single histogram and the intensity represented as a probability density function (the area of each bar equals the probability that a randomly chosen grain size belongs to this bar). It was previously observed[16] that isothermal annealing of zone-refined iron leads to a dispersion of grain sizes that increases with annealing time. The same observation is made in our case even for a different method of grain growth that combines both mechanical and thermal treatment. In the following, we will consider three distributions to describe the histograms in Figures 7(a) and (b). For a wide range of materials, it was shown that log-normal

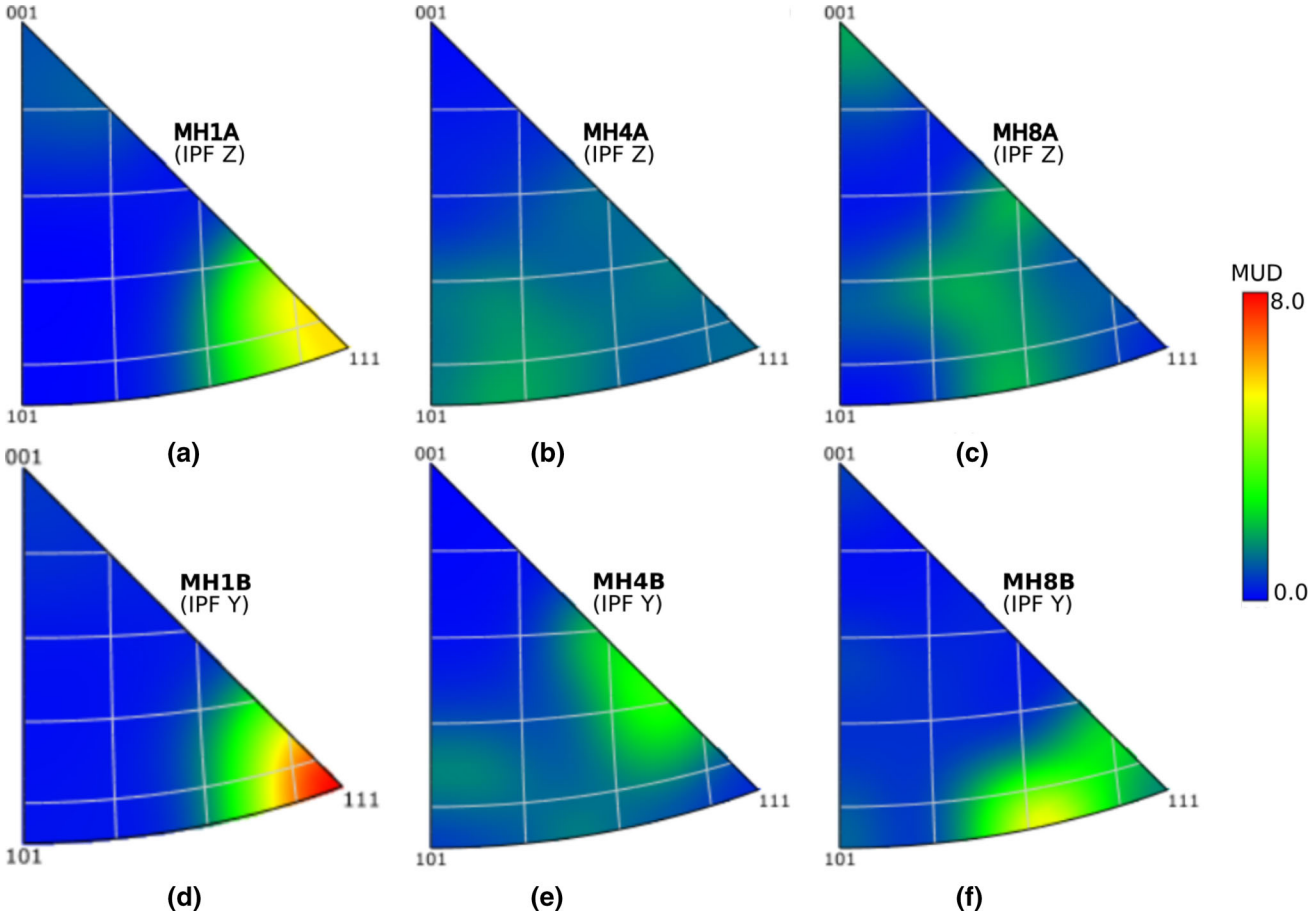

Fig. 6—Inverse pole figures showing the changes in the orientations of grains during a combined mechanical and thermal treatment: (*a*, *d*) sample MH1, (*b*, *e*) sample MH4, (*c*, *f*) sample MH8. The figures in the upper row were taken from the side A, and those in the lower row from the side B of the respective sample. The color scale shows the multiple of uniform density (MUD) that represents a deviation from the mean IPF value measured inside one triangle (Color figure online).

distribution fits the number density quite well.[24] Since the grain diameter is proportional to the chord length (see earlier in this section) and the probability density is just a rescaled number density, we can express the probability density function for the log-normal distribution as

$$p(l) = p_{\mathrm{m}} \exp\left\{-b^2[\log(l/l_{\mathrm{m}})]^2\right\}, \qquad [3]$$

where l_{m} is the most probable chord length (middle of the bar with the highest p in the histogram), p_{m}, b are adjustable parameters, and log is a natural logarithm. The value of $l_{\mathrm{m}} = 0.075$ mm was found to be the same for both samples MH4 and MH8. The fit to our data using Eq. [3] (blue curves in Figure 7) including the measure of the goodness of fit (χ^2; ideally zero) are: $p_{\mathrm{m}} = 3.681$, $b = -0.726$ ($\chi^2 = 0.72$, sample MH4), and $p_{\mathrm{m}} = 2.509$, $b = -0.622$ ($\chi^2 = 0.70$, sample MH8). Recently, Foster[25] has made a detailed theoretical analysis of the log-normal distribution, where he emphasized the need for using the proper randomization of the positions (orientations) of planar cuts. This cannot be easily guaranteed in metallographic samples, where the randomization of planar cuts is made either: (i) using large samples with a single cut made across many grains, or (ii) using serial sectioning, making the linear intercept analysis for each cut, and combining the results to obtain the histogram. Unsurprisingly, deviations from the log-normal distributions were previously observed, as pointed out by Hu.[16] As a remedy, other distributions were proposed over the years that fit the measurements better, but they are merely convenient formulas with less obvious physical meaning. In the following, we consider two of them which have received the most attention.

In particular, Aboav and Langdon[26] showed that the log-normal distribution cannot represent the measurements of grain diameters on annealed samples of α-iron. A significantly better agreement was obtained if the logarithm of the number of grains in each bin was related to the square root of the grain diameter, *i.e.*,

$$p(l) = p_{\mathrm{m}} \exp\left\{-\alpha^2\left[\sqrt{l/l_{\mathrm{m}}} - 1\right]^2\right\}, \qquad [4]$$

where p_{m}, α are adjustable parameters. The fit to our data using this distribution is shown in Figure 7 in red, where the coefficients are: $p_{\mathrm{m}} = 3.221$, $\alpha = 0.893$ ($\chi^2 = 0.24$, sample MH4), and $p_{\mathrm{m}} = 2.186$, $\alpha = 0.709$

($\chi^2 = 0.92$, sample MH8). One can immediately observe that this distribution underestimates the peak height of the histogram in Figure 7(a) as well as the peak height and the tail of the distribution in Figure 7(b). Hu[16] has noted the ill-defined limit of this distribution, where the number of grains does not become zero as the grain diameter vanishes. He proposed a modification of this distribution, which removes this drawback and simultaneously reproduces the measured grain size distributions more closely than the log-normal distribution:

$$p(l) = A\, l \exp\left\{-a^2 (l/l_m)^2\right\} \qquad [5]$$

with A, a being the adjustable parameters. The fit to our data using this distribution is shown in Figure 7 in green, where the fitted parameters are: $A = 41.794$, $a = -0.386$ ($\chi^2 = 4.70$, sample MH4), and $A = 32.505$, $a = -0.405$ ($\chi^2 = 6.02$, sample MH8). Comparing the values of χ^2 obtained for individual distributions clearly shows that Eq. [5] is the worst choice irrespective of how the sample was treated.

Comparing the values of χ^2 above, one sees that our measurements on sample MH4 are best reproduced by the square-root distribution (Eq. [4]) whereas the data on sample MH8 are described better using the log-normal distribution (Eq. [3]). The slightly better fit of the data for MH4 using the square-root distribution was expected, because this sample was treated in a similar way as in previous experiments studying the effect of annealing times on grain size distributions, where the log-normal distribution was found inapplicable (see Hu[16] for details). However, repeated application of cold work and annealing results in significant broadening of the grain size distribution as shown in the tail of the histogram in Figure 7(b). Here, only the log-normal distribution provides the necessary curvature to simultaneously fit the data at small and large grain sizes.

All three grain size distributions above are based on the approximation of individual grains by spheres. On the theoretical level, a more detailed analysis of grain growth is possible within phase field models[27] which provide simultaneous orientations of grain sizes and shapes. A direct imaging of grains is now possible using the three-dimensional X-ray diffraction microscopy on synchrotrons, as proposed and demonstrated by Schmidt and co-workers.[28–31] These experiments open the possibility to further advance the models linking the properties of planar cuts to three-dimensional distributions of grains inside the material. An extension of these measurements was proposed recently by Sun *et al.*[32] which allows to simulate temporal changes in the distribution of grain sizes and shapes. A new technique to grow iron single crystals from a lithium-rich melt was used recently by Fix *et al.*[33] which simplifies the

Table II. The Average Grain Volumes V_g Calculated from the EBSD Maps on Samples MH4 and MH8 (Figs. 3 and 4) Using the Linear Intercept Method by Eq. [2]

Specimen	Side	V_g (mm^3)	d (mm)	$\overline{d}$ (mm)
MH4	A	0.002	0.223	0.348
	B	0.005	0.311	0.370
MH8	A	0.050	0.669	0.736
	B	0.070	0.749	0.857

The characteristic grain sizes d and $\overline{d}$ were obtained by two different methods as explained in the text.

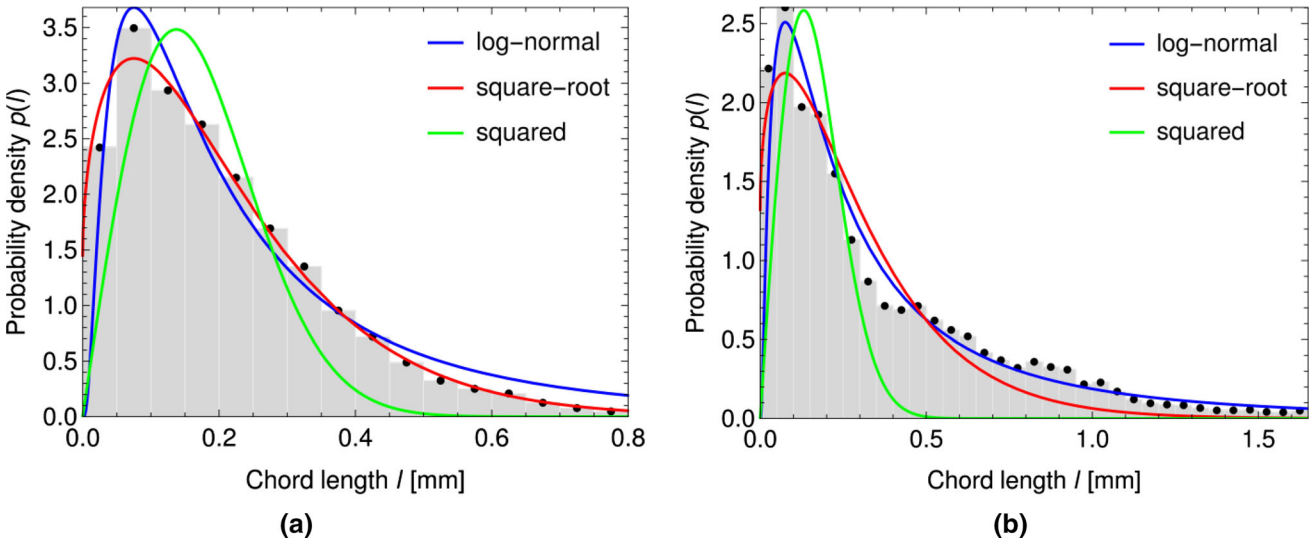

Fig. 7—Distribution of probability densities of chord lengths calculated on samples (*a*) MH4, and (*b*) MH8. The histograms were created from the data obtained by placing 15,000 randomly oriented lines over the sides A and B and combining the data from both sides. This leads to better randomization of the positions of planar cuts as explained in the text. The widths of bars in both plots are 0.05 mm. The mathematical representations of the three distribution functions used to fit our data are given in the text: log-normal (Eq. [3]), square-root (Eq. [4]), squared (Eq. [5]) (Color figure online).

synthesis of iron single crystals for further mechanical testing. The samples produced this way contained 90 ppm of nitrogen, but no formation of iron-nitride precipitates was observed.

IV. CONCLUSIONS

The objective of this paper was to determine the optimal combination of mechanical and thermal treatment of electrolytic iron with columnar grains so as to maximize the grain size. The best results were obtained by using four cycles of cold work at room temperature followed by annealing at 870 °C for 8 hours (our sample MH8). The EBSD analysis on this sample revealed that some grains are larger than 2 mm, whereas theoretical estimates of the average grain size give values between 1 and 1.5 mm. The grains produced by our procedure are much bigger than those achieved by Kadečková and Šesták[6] who used polycrystalline iron with approximately spherical (polyhedral) grains. This observation suggests that the room-temperature deformation of columnar microstructures is more effective in producing internal strain and the ensuing dislocation networks have larger capacity in driving the abnormal grain growth.

The linear intercept method was used to obtain the distribution of grain sizes in two samples—one after a single cold work and optimal annealing time (MH4) and the other after the optimal combination of cold work and annealing cycles (MH8). In the former case, the probability density function of chord lengths is not log-normally distributed, but its logarithm is slightly better approximated by the squares-root of chord lengths. However, a repeated application of cold work and annealing induces the growth of larger grains, which makes the tail of the distribution more statistically significant. In this case, the probability density of chord lengths becomes log-normally distributed as in grain growth experiments on most other metals.

The final samples obtained by the procedure developed here are still polycrystalline, but the microstructure is extremely coarse-grained. The sizes of larger grains are well above the 1.5 μm threshold above which the experiments on micropillars exhibit bulk-like response.[34] The plastic deformation of these coarse-grained polycrystals will thus be dominated by the slip activity inside individual large grains. This opens the possibility to study a variation of the mechanism of plastic deformation of iron single crystals with the orientation of the applied load by straining a single specimen. Similarly, *in situ* nanoindentation can be used to probe the response of individual large grains while avoiding the effects of grain boundaries. Large micropillars can be prepared by focused ion beam technique from large grains of a number of different orientations, and subjected to *in situ* straining experiments in SEM.

ACKNOWLEDGMENTS

The authors thank Dr. Jiří Svoboda for fruitful discussions on the strain anneal technique. This research was supported by the Czech Science Foundation, Grant No. 19-23411S. J.H. acknowledges financial support from the Ministry of Transport within the programme of long-term conceptual development of research institutions. Infrastructure of the CEITEC Nano Research Centre was utilized for the measurements made in this work.

DATA AVAILABILITY

The data used to support the findings of this study are available from the corresponding author upon request.

CONFLICT OF INTEREST

The authors declare to have no conflicts of interest.

REFERENCES

1. M.E. Hermant: *Acta Metall.*, 1968, vol. 16, pp. 1–6.
2. H.K.D.H. Bhadeshia and R. Honeycombe: *Steels—Microstructure and Properties*, 3rd ed. Butterworth-Heinemann, Oxford, 2006, pp. 1–6.
3. H.C.H. Carpenter: *Nature*, 1926, vol. 118, pp. 266–69.
4. G. Mayer and W.A. Backofen: *Mater. Res. Bull.*, 1967, vol. 2, pp. 871–75.
5. C. Antonione, F. Marino, G. Riontino, and M.C. Tabasso: *J. Mater. Sci.*, 1977, vol. 12, pp. 747–50.
6. S. Kadečková and B. Šesták: *Krist. Tech.*, 1967, vol. 2, pp. 191–203.
7. S. Kadečková and K.Z. Saleeb: *J. Cryst. Growth*, 1975, vol. 30, pp. 335–42.
8. H.H. Kranzlein, M.S. Burton, and G.V. Smith: *Mem. Sci. Rev. Metall.*, 1968, vol. 65, pp. 361–68.
9. H.E. Rosinger, W.J. Bratina, and G.B. Craig: *J. Cryst. Growth*, 1970, vol. 7, pp. 42–44.
10. D.S. Tomalin and C.J. McMahon Jr.: *Mater. Sci. Eng.*, 1971, vol. 8, pp. 54–56.
11. D.J. Bailey and E.G. Brewer: *Metall. Trans. A*, 1975, vol. 6, pp. 403–08.
12. K. Lubitz and G. Göltz: *Appl. Phys.*, 1979, vol. 19, pp. 237–39.
13. S. Jin, B. Kang, T. Kong, S.H. Hong, H.J. Shin, and R.S. Ruoffo: *J. Alloys Compd.*, 2021, vol. 853, pp. 157–390.
14. D.R. Almeida, P.R. Rios, D. Zöllner, and H.R.Z. Sandim: *J. Mater. Res. Technol.*, 2020, vol. 9, pp. 11099–11110.
15. Z.W. Zhang, G. Chen, and G.L. Chen: *Acta Mater.*, 2007, vol. 55, pp. 5988–98.
16. H. Hu: *Can. Metall. Q.*, 1974, vol. 13, pp. 275–86.
17. M.J.H. Simmons, P.A. Langston, and A.S. Burbidge: *Powder Technol.*, 1999, vol. 102, pp. 75–83.
18. C.S. Smith and L. Guttman: *J. Met.*, 1953, vol. 5, pp. 81–87.
19. A.W. Thompson: *Metallography*, 1972, vol. 5, pp. 366–69.
20. R.L. Fullman: *Trans. AIME*, 1953, vol. 197, p. 447.
21. J.H. Hensler: *J. Inst. Met.*, 1968, vol. 96, pp. 190–92.
22. G.A. Miller, D.H. Avery, and W.A. Backofen: *Trans. AIME*, 1966, vol. 236, p. 1667.
23. P. Feltham: *Acta Metall.*, 1957, vol. 5, pp. 97–105.

24. F. Schückher: in *Quantitative Microscopy*. R.T. DeHoff and F.N. Rhines, eds., McGraw-Hill Book Co., New York, 1968, pp. 201–65.
25. C.R. Foster: *Metall. Mater. Trans. A*, 2022, vol. 53A. pp. 3507–11.
26. D.A. Aboav and T.G. Langdon: *Metallography*, 1969, vol. 1, pp. 333–40.
27. I.M. McKenna, S.O. Poulsen, E.M. Lauridsen, W. Ludwig, and P.W. Voorhees: *Acta Mater.*, 2014, vol. 78, pp. 125–34.
28. S. Schmidt, S.F. Nielsen, C. Gundlach, L. Margulies, X. Huang, and D. Juul Jensen: *Science*, 2004, vol. 305, pp. 229–32.
29. E.M. Lauridsen, S. Schmidt, S.F. Nielsen, L. Margulies, H.F. Poulsen, and D. Juul Jensen: *Scripta Mater.*, 2006, vol. 55, pp. 51–56.
30. S. Schmidt, U.L. Olsen, H.F. Poulsen, H.O. Sørensen, E.M. Lauridsen, L. Margulies, C. Maurice, and D. Juul Jensen: *Scripta Mater.*, 2008, vol. 59, pp. 491–94.
31. S. Van Boxel, S. Schmidt, W. Ludwig, Y.B. Zhang, D. Juul Jensen, and W. Pantleon: *Mater. Trans.*, 2014, vol. 55, pp. 128–36.
32. J. Sun, A. Lyckegaard, Y.B. Zhang, S.A. Catherine, B.R. Patterson, F. Bachmann, N. Gueninchault, H. Bale, C. Holzner, E. Lauridsen, and D. Juul Jensen: *IOP Conf. Ser. Mater. Sci. Eng.*, 2017, vol. 219, p. 012039.
33. M. Fix, H. Schumann, S.G. Jantz, F.A. Breitner, A. Leineweber, and A. Jesche: *J. Cryst. Growth*, 2018, vol. 486, pp. 50–55.
34. B.R.S. Rogne and C. Thaulow: *Philos. Mag.*, 2014, vol. 95, pp. 1814–28.